Future Journal of Pharmaceutical Sciences

RESEARCH Open Access

Xanthine oxidase inhibitory potentials of flavonoid aglycones of *Tribulus terrestris*: in vivo, in silico and in vitro studies

Olusegun Samson Ajala*, Ayotomiwa Olubusayo Ayeleso, Mbang Owolabi, Moshood Olusola Akinleye and Grace Ukpo

Abstract

Background: Despite the ongoing safety-driven spate of flavonoid xanthine oxidase (XOD) inhibition investigations, there is a lack of flavonoid-based uricostatic antihyperuricemic agents in clinical medicine. The poor pharmacokinetic profiles of glycosides (the natural form of existence of most flavonoids) relative to their aglycones could be largely responsible for this paradox. This investigation was aimed at providing both functional and molecular bases for the possible discovery of XOD inhibitory (or uricostatic) anti-hyperuricemic flavonoid aglycones from the leaves of a flavonoid-rich medicinal plant, *Tribulus terrestris*. To this end, the flavonoid aglycone fraction of *T. terrestris* leaf extract (FATT) was evaluated in vivo for antihyperuricemic activity in ethanol-induced hyperuricemic mice, monitoring serum and liver uric acid levels. Molecular docking and molecular dynamics simulation studies were carried out on the three major flavonoid aglycones of *T. terrestris* (isorhamnetin, quercetin and kaempferol) against an inhibitor conformation XOD model. The three flavonoids were also subjected to in vitro XOD activity assay, comparing their IC_{50} to that of allopurinol, a standard uricostatic antihyperuricemic drug.

Results: FATT significantly lowered serum uric acid ($p < 0.0001$) and liver uric acid ($p < 0.05$) levels of the experimental animals, implying anti-hyperuricemic activity with uricostatic action mechanism allusions. Molecular docking studies revealed high binding affinity values (− 7.8, − 8.1, − 8.2 kcal/mol) for the aglycones (isorhamnetin, quercetin and kaempferol, respectively). Radius of gyration and RMSD analyses of the molecular dynamics simulation trajectories of the three aglycone–XOD complexes revealed substantial stability, the highest stability being demonstrated by the kaempferol–XOD complex. In vitro XOD activity assay showed kaempferol (IC_{50}: 8.2 ± 0.9 µg/ml), quercetin (IC_{50}: 20.4 ± 1.3 µg/ml) and isorhamnetin (IC_{50}: 22.2 ± 2.1 µg/ml) to be more potent than allopurinol (IC_{50}: 30.1 ± 3.0 µg/ml).

Conclusion: This work provides a scientific basis for the use of *T. terrestris* in the treatment of hyperuricemia-related (e.g. kidney stone and gout) disorders. It also provides the molecular basis for a focussed screening of the flavonoid aglycones chemical space for the possible discovery of flavonoid-based uricostatic anti-hyperuricemic drugs or drug templates.

Keywords: In silico drug discovery, Flavonoid aglycones, Hyperuricemia, Xanthine oxidase inhibition

Background

Hyperuricemia (HUA), characterized by serum uric acid (SUA) concentration greater than 7 mg/dl, is caused by hepatic overproduction and/or renal underexcretion of uric acid (UA) [1] resulting in the deposition of UA at the joints and kidneys; manifesting

*Correspondence: olajala@unilag.edu.ng

Department of Pharmaceutical Chemistry, Faculty of Pharmacy, CMUL Campus, University of Lagos, PMB 12003, Idiaraba, Surulere, Lagos, Nigeria

Springer Open

© The Author(s) 2022. **Open Access** This article is licensed under a Creative Commons Attribution 4.0 International License, which permits use, sharing, adaptation, distribution and reproduction in any medium or format, as long as you give appropriate credit to the original author(s) and the source, provide a link to the Creative Commons licence, and indicate if changes were made. The images or other third party material in this article are included in the article's Creative Commons licence, unless indicated otherwise in a credit line to the material. If material is not included in the article's Creative Commons licence and your intended use is not permitted by statutory regulation or exceeds the permitted use, you will need to obtain permission directly from the copyright holder. To view a copy of this licence, visit http://creativecommons.org/licenses/by/4.0/.

primarily as gout and kidney stone-related disorders, respectively [2]. In addition, a number of non-stone-forming but grave metabolic conditions like hypertension, type II diabetes, cardiac disorders, etc., have been implicated as functions of HUA, though the extent to which SUA is an independent variable in each is yet unknown [3].

HUA treatment is mainly by SUA lowering, achieved by UA renal excretion enhancement (uricosuric) and/or its biosynthetic inhibition (uricostatic) mechanisms [4]. UA biosynthesis in man and other uricase-deficient animals [5] occurs as the last stage of purine metabolism, involving enzymatic conversion of hypoxanthine to UA via xanthine as an intermediate [6]. This two-stepwise bioconversion is catalysed by the enzyme xanthine dehydrogenase (XDH) which is in dynamic equilibrium with and, hence, readily interconverted to its isoform, xanthine oxidase (XOD). XDH and XOD are, therefore, variants of the same gene product, by virtue of which they are structurally and functionally similar, differing only in the nature of the final electron acceptor required for their redox activities. While the dehydrogenase utilizes the coenzyme nicotinamide adenine dinucleotide (NAD^+) as the final electron acceptor, the oxidase makes use of molecular oxygen for the same purpose [7, 8]. And though they are both independently capable of carrying out the UA biosynthetic statutory function, XOD appears to be the physiological form of the isozyme pair, being the one called to duty during physical exertion [8, 9]. Nevertheless, given the 100% sequence homology in their substrate-binding domains, their catalytic activities cannot be distinguished [9]. In the real sense, therefore, this investigation is essentially representative of flavonoid inhibition of the XDH/XOD isomeric pair and not just of XOD that it, for simplicity, implies.

X-ray crystal structure shows XOD to be a homodimer (Fig. 1A), each subunit comprising three distinct domains as follows: A relatively small N-terminal domain, containing two iron–sulphur centres; the flavin adenine dinucleotide (FAD)-containing domain, which is middle-placed both in position and size and the largest C-terminal domain, containing dioxothiomolybdenum (iv) ion and molybdopterin cofactors [9]. The binding pocket of the enzyme's active site is located in the C-terminal domain (Fig. 1B) of each subunit and consists of its two cofactors' binding regions and the substrate's binding site in which competitive inhibitors also expectedly bind [8, 9]. So far, only three clinical drugs (allopurinol, febuxostat and topiroxostat) [10] are known to inhibit XOD by binding at its active site, disrupting its binding with the substrates, xanthine and hypoxanthine, and their ultimate catalytic conversion to uric acid to elicit SUA lowering. They have found modest applications in the management of acute gout attack and urolithiasis [10], but their prophylactic or routine employment in the management or prevention of non-stone forming HUA-linked metabolic diseases like hypertension and type II diabetes is deterred by their associated severe unwanted effects including Steven Jones syndrome, hepatotoxicity, bone marrow suppression and urticaria [11]. There is therefore a high need for the discovery of new but safer uricostatic anti-hyperuricemic agents.

Flavonoids are a group of natural products that have been investigated for the possible discovery of new and safer XOD-inhibiting anti-hyperuricemic agents, the motivating factor being a general safety notion associated with them on account of their ubiquity in foods, fruits and vegetables, which are freely consumed by animals and humans alike [12]. However, there is yet no flavonoid-based uricostatic agent in clinical medicine. This

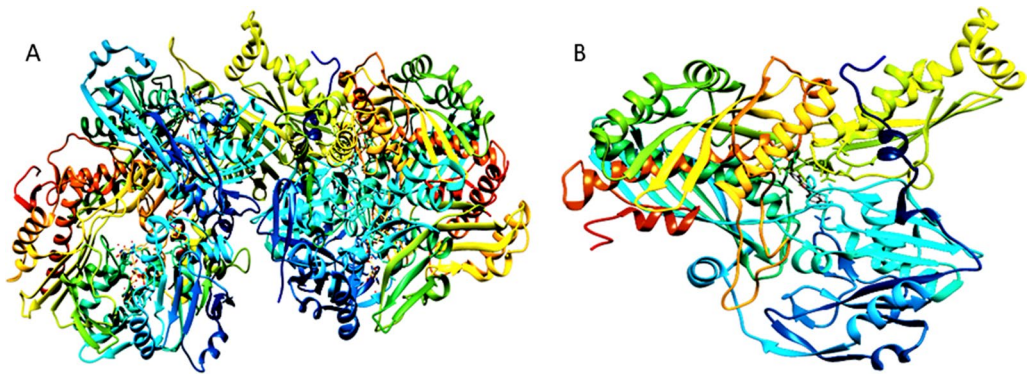

Fig. 1 X-ray crystal structure of **A**: Bovine milk xanthine oxidase homodimer and **B**: C-terminal domain of one of its monomers. Chimera 1.4 was used to remove five of the six chains of the homodimer, leaving only one of its two C-terminal domains used for in silico studies. (PDB ID 3NVY, 2.00 Å)

paradoxical dearth of clinical flavonoid-based uricostatic antihyperuricemics could be attributed, at least, partly to the poor pharmacokinetics profiles of glycosides, the natural form of existence of most flavonoids [13]: In this form, they are poorly orally bioavailable due to poor lipophilicity. In addition, they are highly susceptible to plasma protein binding and metabolically unstable [13]. Bearing the gastric acid hydrolytic activity of the human gut in mind, the therapeutic properties of most glycosidic natural products, flavonoids inclusive, are therefore attributable to their products of acid hydrolysis—their respective aglycones. Hence, the interest in the flavonoid aglycones of the flavonoid-rich plant is of focus in this investigation, *T. terrestris*.

Tribulus terrestris (TT) is an annual plant of Mediterranean origin but is now of global distribution [14, 15]. It has a wide range of folkloric medicinal uses including the treatment of gout, kidney stone and other HUA-related diseases like hypertension, stroke and type II diabetes [15, 16]. It is rich in alkaloids, flavonoids, saponins and the aglycones of saponins (i.e. sapogenins) and flavonoids [16]. So far, the flavonoids obtained from various parts of TT revolve round just three flavonol aglycone skeletons, namely quercetin, isorhamnetin and kaempferol (Fig. 2) [17, 18].

Aim of the study

This study was aimed at evaluating the anti-hyperuricemic potentials of a flavonoid aglycone-rich fraction of *T. terrestris* leaf extract in vivo in mice and to provide structure-based molecular frameworks for its XOD inhibitory action mechanism via molecular docking and molecular dynamics simulations, validating all XOD-flavonoid interactions by an in vitro enzyme activity assay with the aid of commercially available Bovine XOD and pure isorhamnetin, quercetin and kaempferol with an ultimate view to providing functional and molecular platforms for the possible discovery of flavonoid-based uricostatic antihyperuricemic drug leads.

Methods

Tribulus terrestris leaf material and its crude extract

Tribulus terrestris (TT) leaves were purchased from the herb market at Mushin, Lagos, and authenticated at the botany department of the University of Lagos, where a herbarium sample was also deposited with the voucher number LUH7128. The leaves were subsequently dried under shade and pulverized. The pulverized leaf material (800 g) was macerated in methanol (2 L) for 2 days. The extract was decanted and filtered, and its mac was subjected to further maceration in methanol (2 L) for 1

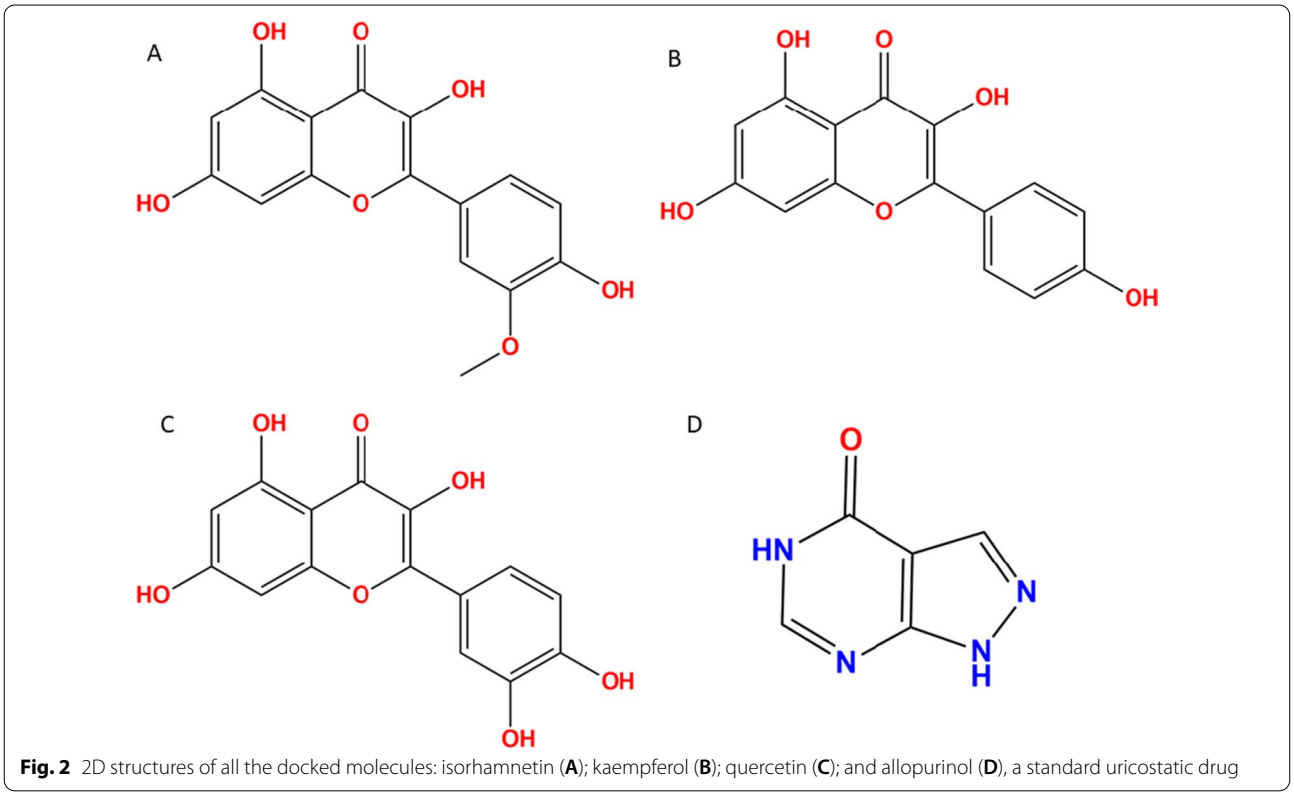

Fig. 2 2D structures of all the docked molecules: isorhamnetin (**A**); kaempferol (**B**); quercetin (**C**); and allopurinol (**D**), a standard uricostatic drug

day. Extracts were bulked and concentrated to dryness *in vacuo* at 40 °C to obtain a dried crude extract (40 g).

Experimental animals

Male albino mice weighing 20–27 g were obtained from the College of Medicine, University of Lagos (CMUL) animal house. They were maintained at standard conditions with a regular diet and water supplied ad libitum. All animal experimental procedures were approved by the Lagos Health Research Ethics committee of the CMUL (#CMUL/ACUREC/08/22/1076).

Materials for uric acid analysis and in vitro XOD inhibition assay

Uricase-based uric acid assay kit by Biolabo$^{R™}$ [19] was used. It is essentially made up of: (1) an enzyme mixture (uricase and peroxidase); (2) a buffer and chromogen mixture and (3) a 10 mg/dl standard solution of uric acid. Absorbance (OD) of chromophore, resulting from the enzymes' activities, was measured using a Cary 50 UV–Vis spectrophotometer. Bovine xanthine oxidase (XOD), pure isorhamnetin, quercetin and kaempferol were obtained from Sigma-Aldrich (Germany).

In silico experimental materials

An HP ProBook equipped with intel Core i5, 500 GB Hard Disk, 8 GB RAM and WiFi was the main hardware; UCSF Chimera 1.14 [20] was used for protein preparations; active site interactions simulations and visualizations were done with the aid of BIOVIA Discovery studio visualizer 2021[21]; multiple-ligand docking was carried out with the PyRx molecular docking software equipped with AutoDock Vina and Open Babel plugins [22]; molecular dynamics simulations were performed using the University of Arkansas for Medical Sciences (UAMS) simlab WebGro web server [23]; other bioinformatics web servers visited for information and downloads included RCSB Protein Databank [24], PubChem [25], CASTp [26], UniProtKB [27] and PRODRG [28].

Flavonoid aglycone-rich fraction of *Tribulus terrestris* leaf extract (FATT) preparation

The dried crude methanol leaf extract of TT (40 g) was triturated with n-hexane, dichloromethane and methanol in succession. The methanol-soluble fraction was concentrated to dryness, yielding 10.0 g of the dried fraction that was later chromatographed on a C18 open column (200 g; 5 × 60 cm), eluting with 50% MeOH and MeOH in succession. The 50% fraction was concentrated to dryness (4.5 g), dissolved in 500 ml of a 1:4 MeOH–2 M HCl mixture, refluxed at 80 °C for 30 min [18] and cooled. After the removal of MeOH under reduced pressure, the ensuing solution was extracted with Dichloromethane (DCM) (350 ml × 3) in a separating funnel to obtain DCM fractions which were bulked, concentrated to dryness *in vacuo* and kept under refrigeration as the flavonoid aglycone fraction of *T. terrestris* leaf extract (FATT). Each of the crude extract and fractions was later screened for the presence of the three dominating phytoconstituents of TT—flavonoids, saponins, and alkaloids [29], using standard methods [30].

Anti-hyperuricemic activity of FATT and its XOD inhibitory action mechanism

Forty-eight male albino mice, weighing 20–27 g per mouse, were randomly sorted into 6 groups (1–6) of eight mice each. Hyperuricemia was induced in five groups (groups 2–6) by a daily oral administration of 50% ethanol at a dose of 1.8 g/Kg body weight for 10 days [31], sparing group 1 (normal group) which received distilled water instead. The following treatments (all by oral administration) were given to the animals an hour after the alcohol or water administration each day: Groups 1 and 2 (normal and negative control groups, respectively) received 5% tween 80 (vehicle); group 3 (positive control group) received 10 mg/Kg allopurinol, while groups 4, 5 and 6 (experimental groups) were, respectively, given 50, 100 and 200 mg/Kg doses of FATT. The animals were killed under anaesthesia on the eighth day to obtain their blood samples by cardiac puncture and have their livers excised. The uric acid content of the blood and liver samples was determined and correlated with anti-hyperuricemic and XOD inhibitory activities, respectively.

Analysis of UA in blood and liver samples

Each blood sample was allowed to clot and then centrifuged at 3000 × g for 5 min. One millilitre of the supernatant (serum) was used for subsequent analysis. On the other hand, harvested liver from each animal (about 1.30 g, on average) was homogenized in 1 ml of ice-cooled phosphate buffer (pH 7.4) and centrifuged at 12,000 × g for 5 min and the supernatant used for subsequent analysis [32, 33].

UA analysis of the blood serum and liver homogenate samples was carried out according to procedures prescribed in the Biolabo$^{R™}$ uric acid assay kit manual [19], with little modifications. The analysis predicated on colorimetric principles as follows: Assay kit's reagents R1 and R2 were mixed to produce a working reagent mixture containing uricase, peroxidase and a chromogen built with aminoantipyrine and dichlorohyroxybenze sulphonate precursors [34]. Twenty-five microlitres of the sample (serum or liver homogenate) was added to 1000 µl of the working reagent mixture and incubated for 5 min at room temperature to allow uricase act on uric acid in the sample to produce allantoin, carbon dioxide

and hydrogen peroxide which, in the presence of peroxidase, acted on the earlier formed chromogen to produce quinoneimine, a red-coloured complex. The absorbance of the complex in the final mixture was measured (using a Cary 50 UV–Vis spectrophotometer at 505 nm wavelength) and correlated with the sample's uric acid concentration. The procedure was repeated for the assay kit's reagent R3 (a 10 mg/dl UA standard solution), and the sample concentration was calculated using the formula:

$$\text{Conc.} = \frac{\text{Abs. Sample}}{\text{Abs. Standard}} \times 10\left(\text{mg/dl}\right)$$

For the liver samples, UA concentration in mg/dl of homogenate was converted to mg/g of liver, using the liver weight homogenized.

In vitro XOD inhibition assay

Experimental details of the assay followed established procedures [35, 36] with little modifications as follows: Bovine milk XOD (Sigma-Aldrich) was incubated in the presence of xanthine with varying concentrations (5–100 µg/ml) of each of isorhamnetin, quercetin, kaempferol and allopurinol (standard) prepared in 5% DMSO; enzyme activity was measured as the uric acid concentration of the reaction mixture and monitored as absorbance at 290 nm with a UV–Visible spectrophotometer. The assay mixture was prepared with 1 ml of the solution of the test substance, 2.9 ml of phosphate buffer (pH 7.5) and 0.1 ml of the xanthine oxidase enzyme solution (0.1 units/ml in a pH 7.5 phosphate buffer), prepared immediately before use. After allowing for a pre-incubation period of 15 min at 25 °C, the reaction was initiated by the addition of 2 ml 150 µM xanthine solution (prepared in the phosphate buffer) and the assay mixture was incubated at 25 °C for 30 min. The reaction was then stopped by the addition of 1 ml of 1 N HCl and the absorbance was measured at 290 nm. The assay was done in triplicates, and the mean percentage inhibition was calculated by the following equation. IC_{50} values were subsequently determined from the percentage inhibition data [32, 33].

$$\text{Inhibition}(\%) = \left(\frac{(A-B)-(C-D)}{(A-B)}\right) \times 100$$

where A = absorbance of mixture of enzyme, substrate and buffer (without test substance) after incubation; B = absorbance of mixture of substrate and buffer (without the enzyme and test substance) after incubation; C = absorbance of mixture of enzyme, substrate, buffer and test substance after incubation; D = absorbance of mixture of enzyme and buffer (without substrate and test substance) after incubation.

Pre-docking protein and ligands preparations

The X-ray crystal structure of bovine milk XOD homodimer complexed with quercetin (PDB ID 3NVY; resolution 2.00 Å) was uploaded into Chimera 1.14 workspace by direct fetch from the Protein Databank (PDB). Chain C of the six (A, B, C, J, K, L) chains of the homodimer was selected, and the others were deleted. All non-standard residues comprising dioxothiomolybdenum (iv) ion, molybdopterin and water molecules were removed. Hydrogens and AMBER charges were added followed by energy minimization using 200 steepest descent and 10 conjugate gradient steps. The prepared protein structure was saved as a pdb file for subsequent uses. The 3D structures of the three flavonoid aglycones of interest (quercetin, isorhamnetin and kaempferol) were downloaded as structure data files (sdf) from PubChem along with that of allopurinol, a standard uricostatic drug. The downloaded structures were uploaded into the Open Babel plugin workspace of the PyRx docking software for energy minimization and their subsequent conversion into AutoDock-compliant (or pdbqt) ligands.

Multiple ligands docking and docking validation

The prepared protein was uploaded into the PyRx docking workspace and made macromolecule. The docking site was mapped using the active site amino acid residues information obtained from the Computed Atlas of Surface Topography of proteins (CASTp) and UniProt web servers. Multiple-ligand docking algorithm was run using the Vina plugin with its characteristic rigid-macromolecule–flexible-ligand features, ligand degree of freedom being fixed at 8 to produce a maximum of 9 conformational models per ligand. With the understanding that quercetin was also the co-crystallized ligand, making its docking more or less a redocking process, the coordinates of its most stable (or best docking pose) were superimposed on those of its XOD co-crystallized structure, calculating variations between atoms of the two conformations as root-mean-square deviation (RMSD) by the BIOVIA Discovery Studio visualizer software.

Molecular dynamics simulations of aglycone–XOD complexes

The three aglycone–XOD complexes were subjected to molecular dynamics simulation to evaluate their stability in the rather dynamic physiological environments using WebGro, the University of Arkansas for Medical Sciences (UAMS) web server for molecular dynamics simulations, with the following independent variables set as parameters: Box type was triclinic with SPC water model; GROMOS9643a1 was selected as force field; equilibrium temperature was 300 K, while simulation time was set at

20 ns. Ligand–protein complexes pdb files were prepared with BIOVIA Discovery Studio 2021; ligand topology files were prepared with the PRODRG web server, using Microsoft notepad to transfer ligand coordinates from ligand–protein complex pdb files to the PRODRG workspace, validating calculations with correct 3D structure generated by the web server from the coordinates inputs; trajectory analysis was limited to root-mean-square deviation (RMSD) and radius of gyration (Rg) plots [23, 37].

Results

Phytochemical screening of crude extract and fractions of TT leaf extract

The distribution of the three major phytochemical groups (alkaloids, flavonoids and saponins) of TT is given in Table 1. The three were present in the crude extract but unequally distributed in the fractions.

Serum uric acid (SUA)-lowering effects of *Tribulus terrestris* of FATT

SUA level of the hyperuricemic group (negative control) was significantly higher than that of the normal control group ($p < 0.0001$) (Fig. 3). Each of the three doses (50, 100 and 200 mg/Kg) of the flavonoid aglycone fraction of *T. terrestris* leaf extract (FATT) showed highly significant SUA-lowering effects compared to the negative control ($p < 0.0001$). There was no clear dose dependence pattern of FATT anti-hyperuricemic effect at this dose range as depicted in Fig. 3.

Liver uric acid (LUA)-lowering effects of FATT

The liver uric acid (LUA) level of the hyperuricemic (negative control) group was significantly higher than that of the normal control ($p < 0.001$) though not as much as that observed for SUA ($p < 0.0001$). Similarly, the flavonoid aglycone fraction did not show as much LUA-lowering effect as its SUA lowering, the only significant lowering ($p < 0.05$) showing at the highest FATT dose, 200 mg/Kg (Fig. 4).

Docking validation

Re-docked quercetin superimposed on its co-complexed conformation with an RMSD of 1 Å. Figure 5 depicts the structural representation of the superimposed coordinates of the co-complexed and re-docked quercetin molecules.

Xanthine oxidase (XOD) binding affinities of flavonoid aglycones

Quercetin docking served as validation docking, giving a binding energy of − 8.1 kcal/mol. All the docked flavonoid aglycones of *T. terrestris* were observed to show higher binding affinities (or lower binding energies) than that of allopurinol, a standard and pioneer uricostatic anti-hyperuricemic agent. These observations are summarized in Table 2.

Active site interactions of allopurinol and the three flavonoid aglycones of TT

Allopurinol was observed to be in a completely different orientation than the three flavonoid aglycones in the XOD active site, thereby interacting with completely different active site residues than the ones the aglycones showed interactions with: For instance, each of the aglycones showed a pi-alkyl interaction with the substrate-binding ARG912, isorhamnetin showing additional carbon–hydrogen interaction with the catalytic GLU802. On the other hand, allopurinol's interactions were a conventional hydrogen bond with THR 1093 and a pi-sigma bond with GLN1040 (Figs. 6, 7, 8 and 9).

Molecular dynamics simulations of aglycone–XOD complexes

The radius of gyration of each of the aglycone–XOD complexes was largely maintained around 28 Å, and its RMSD was kept below 3 Å in the entire course of 20-ns simulation time. Figures 10 and 11, respectively, depict the radius of gyration and RMSD analyses of the trajectories of the simulations.

Table 1 Relative distribution of the three dominant phytochemical groups of *Tribulus terrestris* in its leaf extract and fractions

Phytochemical	Extract/fraction					
	Crude extract	NH-soluble	DCM-soluble	50% MeOH CFr	MeOH CFr	FATT
Alkaloid	+	−	+	−	−	−
Flavonoid	+	−	+	+	−	+
Saponin	+	−	−	−	+	−

+ = Present; − = Absent

NH n-hexane; *DCM* dichloromethane; *50% MeOH CFr* 50% methanol chromatographic fraction; *MeOH CFr* 100% methanol chromatographic fraction; *FATT* flavonoid aglycone fraction of *Tribulus terrestris* leaf extract

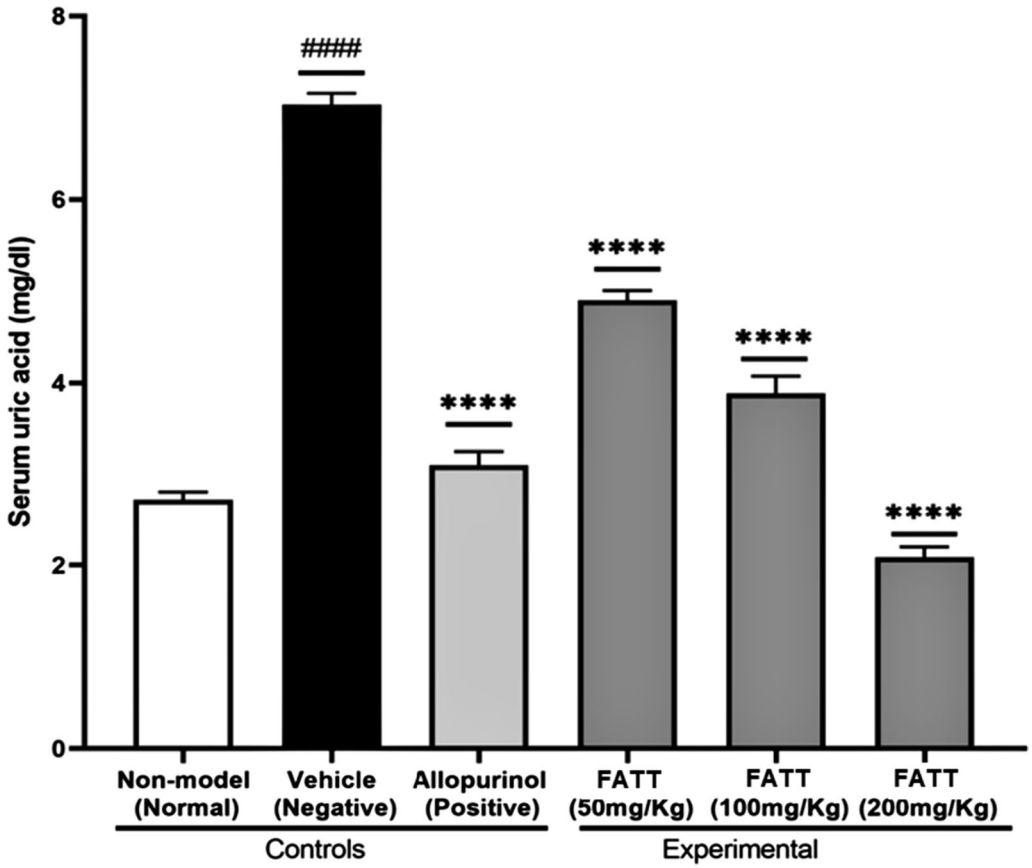

Fig. 3 One-way ANOVA (with Tukey's post hoc) comparison of serum uric acid (SUA) levels of experimental (FATT-treated) and control mice groups. Data are presented as mean ± SEM ($n = 8$); SUA levels of negative and normal controls were compared to ensure SUA elevation before treatment; SUA levels of each of FATT-treated and negative control groups were compared to evaluate FATT's SUA-lowering effects. There was a highly significant SUA elevation before treatment ($^{\#\#\#\#}p < 0.0001$); similarly, there was a highly significant SUA lowering in each of the 50, 100 and 200 mg/Kg FATT-treated groups ($^{****}p < 0.0001$)

In vitro xanthine oxidase inhibition assay

The IC50s of the three flavonoid aglycones and allopurinol are given in Table 3.

Discussions

Hyperuricemia induction

Because hepatic XOD inhibition involvement was crucial to the intended anti-hyperuricemic activity investigation, the induced hyperuricemia would require at least some allusions to hepatic UA biosynthesis contribution. Hence, the adoption of the ethanol induction method depends primarily on the accumulation of purines from excess ATP consumption accompanying ethanol metabolism and its consequent enhanced hepatic XOD bioconversion of purines to UA [38]. This precluded the use of potassium oxonate (PO), commonly employed for hyperuricemia induction in rodents, as its action mechanism, predicated on the rodent-encoded uricase inhibition, hinges on UA urinary elimination impairment with no modicum of hepatic XOD biosynthetic activity contribution [39]. All the same, the suitability of the adopted ethanol induction method was manifest in the significant increases in SUA ($p < 0.0001$) and LUA ($p < 0.05$) levels of the negative control group compared to those of the normal control group (Figs. 3 and 4).

SUA- and LUA-lowering effects of FATT

Each of the three doses of FATT investigated showed a significant SUA-lowering effect compared to the negative control ($p < 0.0001$). While the activity of each dose was comparable to that of allopurinol, no significant dose dependence was observable, probably because the dose range over which such observation could be made had been exceeded. And though this anti-hyperuricemic activity only partly, by virtue of the induction mechanism, alluded to XOD inhibition, it sufficed greatly in establishing the anti-hyperuricemic activity of FATT, thereby providing a strong scientific basis for the application of the

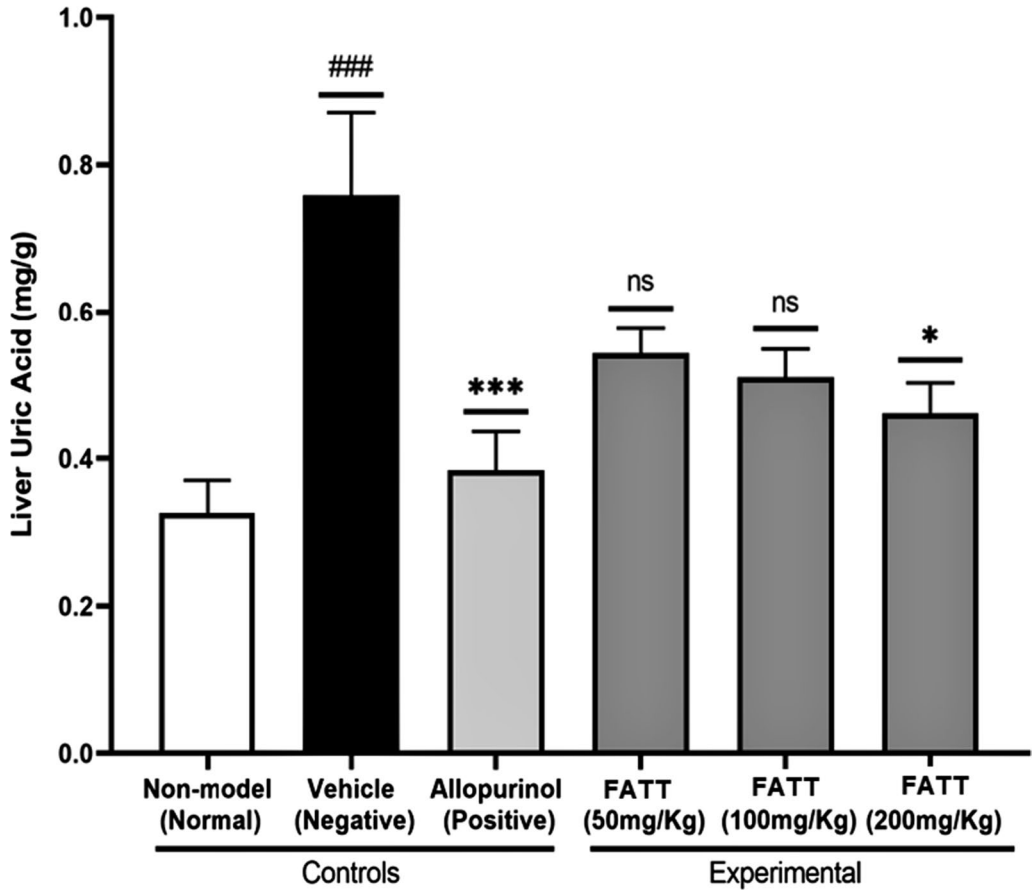

Fig. 4 One-way ANOVA (with Tukey's post hoc) comparison of liver uric acid (LUA) levels of experimental (FATT-treated) and control mice groups. Data are presented as mean ± SEM ($n = 8$); LUA levels of the negative and normal controls were compared to ensure LUA elevation before treatment; LUA levels of each of FATT-treated and negative control groups were compared to evaluate FATT's LUA lowering effects. There was significant LUA elevation before treatment ($^{###}p < 0.001$); there was significant LUA lowering in only the 200 mg/Kg FATT-treated group ($^{*}p < 0.05$)

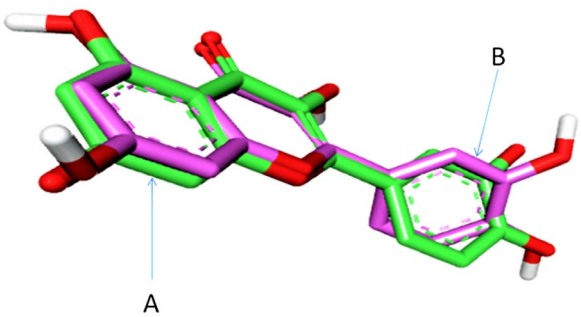

Fig. 5 Stick model superimposition of coordinates of co-crystallized (**A**) and docked (**B**) conformations of quercetin. The two structures were superimposed in the Discovery Studio Visualizer's workspace and RMSD calculated, setting A as reference. The superimposed structures overlaid with a high degree of correspondence, differing only with an RMSD of 1 Å

Table 2 Binding energies (in Kcal/mol) of allopurinol and the three flavonoid aglycones of *Tribulus terrestris* (isorhamnetin, quercetin and kaempferol) with an inhibitor conformation model of xanthine oxidase (XOD)

Ligand	Binding energy (Kcal/mol)
Isorhamnetin	−8.2
Quercetin	−8.1
Kaempferol	−7.8
Allopurinol	−5.9

plant in its earlier-mentioned treatment claims of kidney stone and other hyperuricemia-related disorders in ("Background" section).

A comparison of SUA and LUA data (Figs. 3 and 4) showed that only the highest dose of FATT (200 mg/

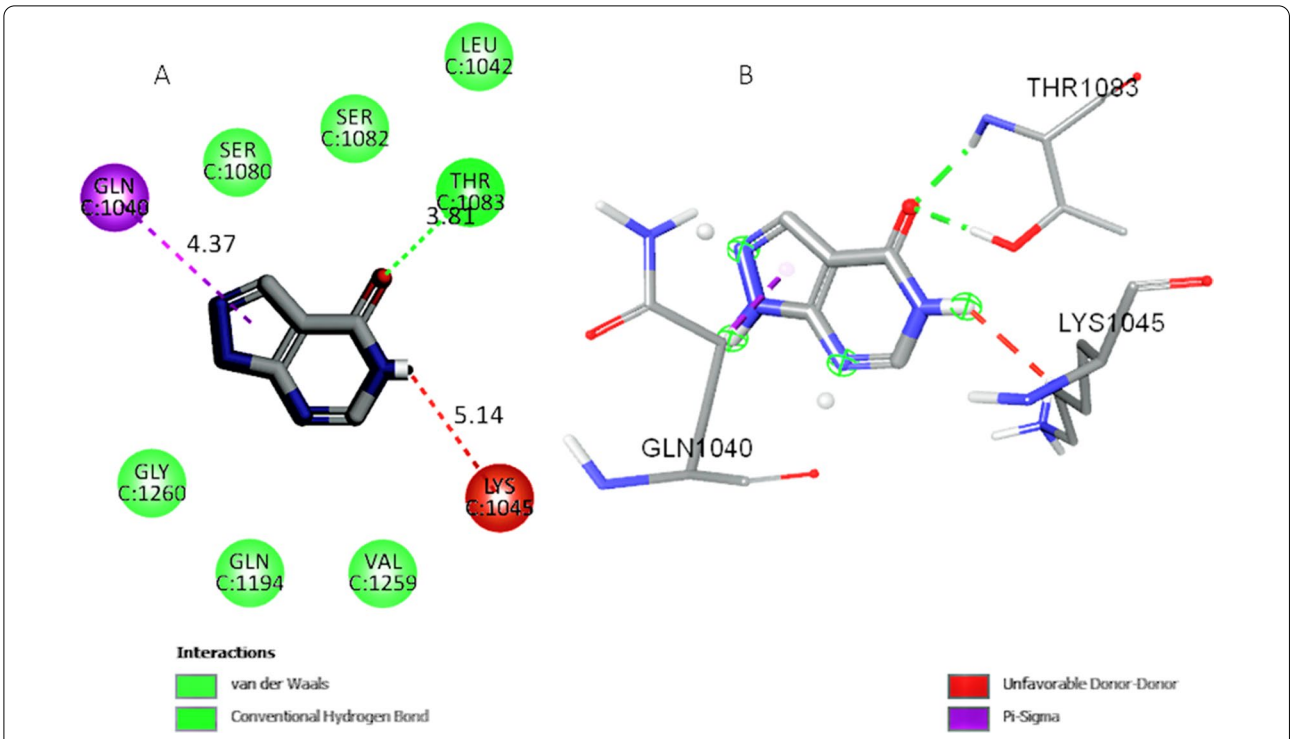

Fig. 6 2D (**A**) and 3D (**B**) simulations of allopurinol–XOD active site supramolecular bondings, showing a conventional hydrogen bond (with THR1093) and a pi-sigma bond interaction (with GLN1040) that are neither of substrate binding nor of catalytic importance

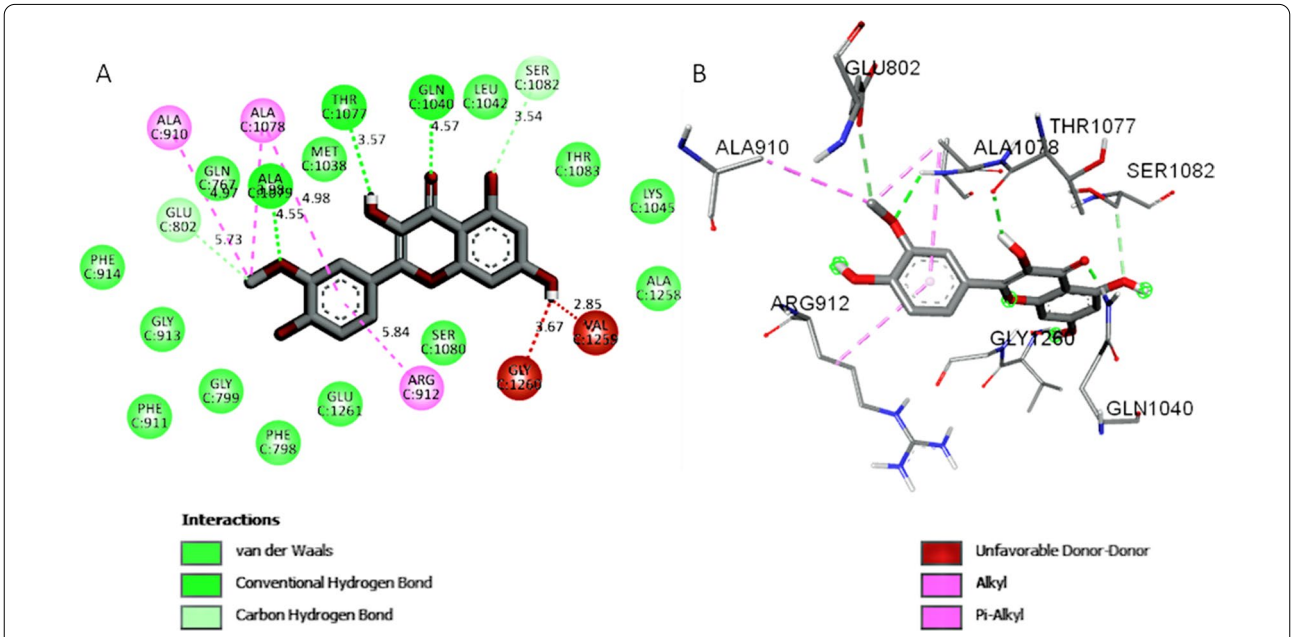

Fig. 7 2D (**A**) and 3D (**B**) simulations of isorhamnetin–XOD active site supramolecular bondings, showing a pi-alkyl interaction with the substrate-binding ARG912 and a carbon–hydrogen interaction with the catalytic GLU802

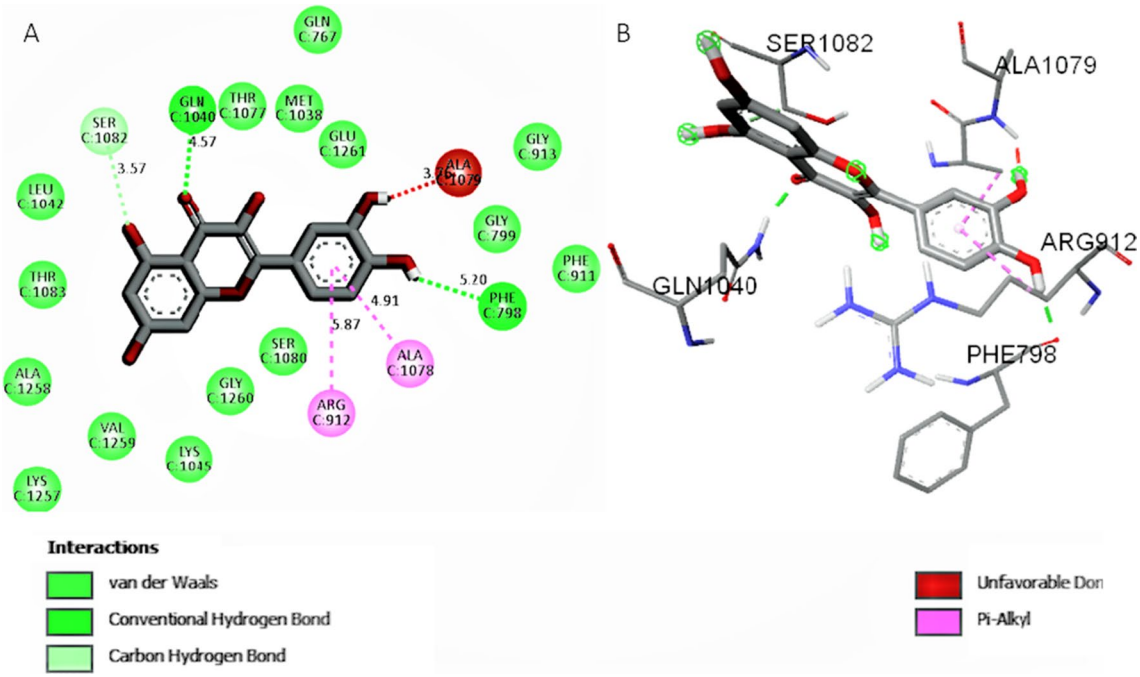

Fig. 8 2D (**A**) and 3D (**B**) simulations of quercetin–XOD active site supramolecular bondings, showing a substrate-binding consequential pi-alkyl interaction with ARG912

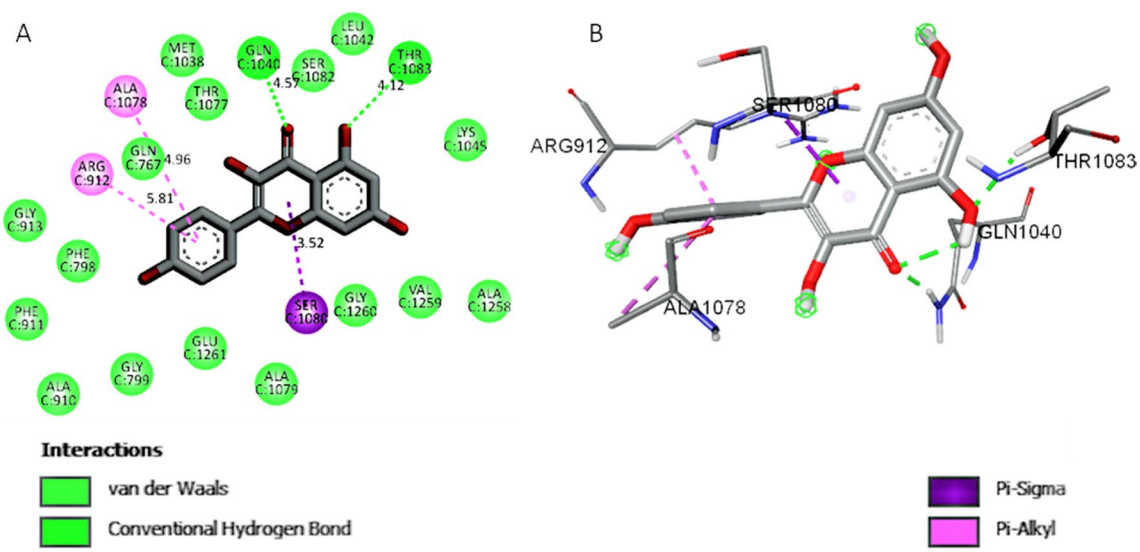

Fig. 9 2D (**A**) and 3D (**B**) simulations of kaempferol–XOD active site supramolecular bondings, showing a substrate-binding consequential pi-alky interaction with ARG912

Kg) produced a significant LUA lowering ($p < 0.05$). A comparison of this p value with that of SUA lowering ($p < 0.0001$) even at the lowest (50 mg/Kg) dose showed FATT demonstrating much greater potency for lowering SUA than for LUA. Notwithstanding, given the fact that LUA accumulation could only have occurred by overwhelming hepatic UA biosynthesis, unlike SUA accumulation, which could occur either as a result of excessive UA biosynthesis and/or its impaired urinary elimination, LUA-lowering data appear more associable

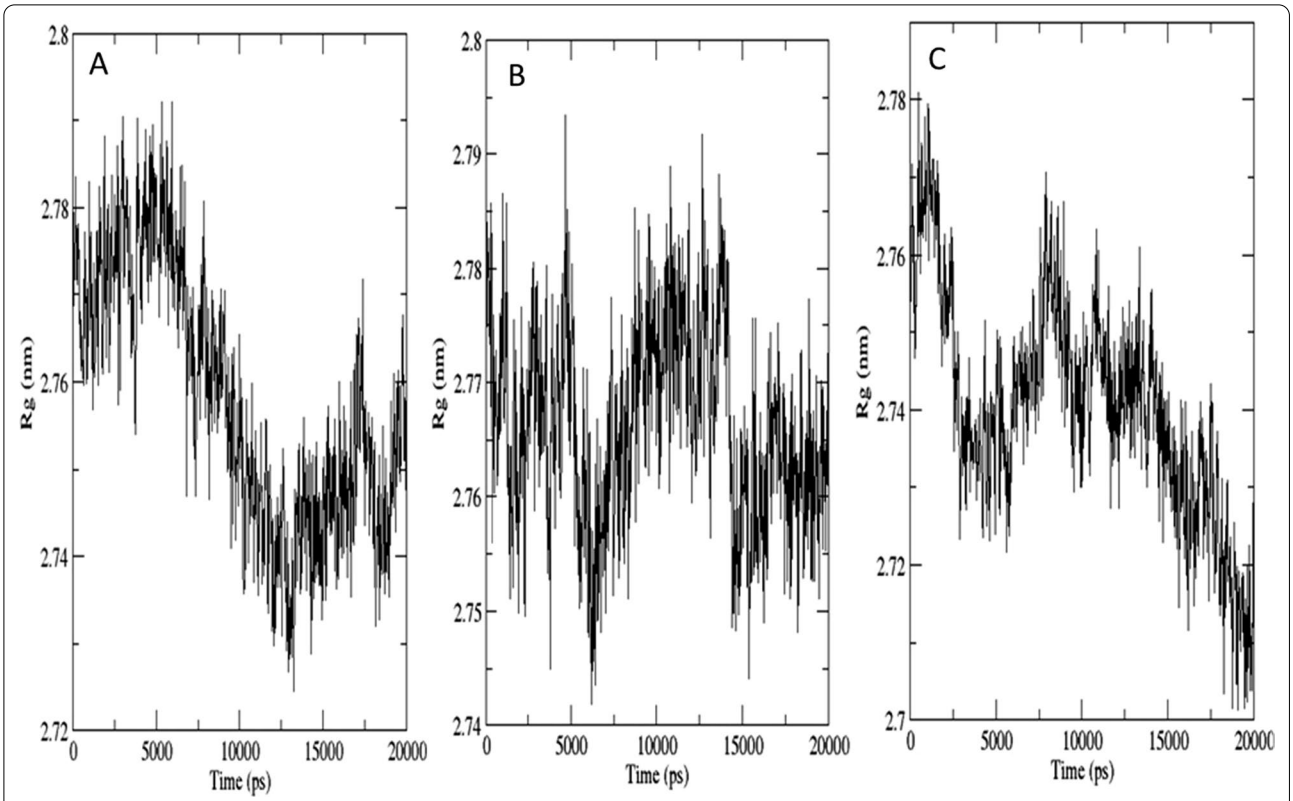

Fig. 10 Radii of gyration of: **A** isorhamnetin–XOD, **B** kaempferol–XOD and **C** quercetin–XOD complexes over a 20-ns simulation time

with hepatic XOD inhibition than do the corresponding SUA data.

However, the huge variation in the intensities of these two responses over the same dose range was indicative of variation in action mechanisms. For instance, the fact that FATT did not show LUA lowering effect at 50 mg/Kg dose, at which its SUA-lowering activity was not only highly significant ($p < 0.0001$) but also above which there was no dose dependency (Fig. 3), showed that the XOD inhibitory SUA-lowering effect of FATT must have been greatly augmented by some additional SUA-lowering means. And recalling that the only known alternative LUA-lowering means is UA urinary elimination enhancement, anti-hyperuricemic effects of flavonoid aglycones could be conjectured as jointly uricostatic and uricosuric.

Xanthine oxidase (XOD) model and chain selection

The unavailability of an inhibitor conformation of the human XOD in the Protein Databank (PDB) at the time of this investigation warranted using the 3NVY-coded XOD model as substitute. It is the X-ray crystal model of bovine milk XOD co-crystallized with a flavonoid inhibitor, quercetin [40]. It should be noted that the factor of primary consideration in this selection was the existence of the protein in its inhibitor conformation, the presence of flavonoid as co-crystallized ligand being merely fortuitous. Additional key considerations in this bovine XOD choice, however, were its mammalian origin and the superimposability of its active site on that of the human enzyme [41, 42]. Moreover, the 3NVY homodimer model was particularly suitable considering its good resolution (2.00 Å) and distinct demarcation of the three domains in each monomer into chains, A B C in one and J K L, respectively, in the other [43]. This enabled the use of only chain C, one of the two active site-containing chains (chains C and L) of the homodimer, for the docking and other in silico studies, making time-involving in silico processes (e.g. protein preparation) achievable within practicable computational time.

Docking validation and binding affinities of the aglycones with XOD

Figure 5, a stick model of the overlay of the coordinates of the co-crystallized quercetin conformation and those of its docked best pose, visually shows excellent correspondence calculated as 1.00 Å RMSD by the Discovery Studio software. The docking protocol was thereby validated.

The binding energies of the three flavonoid aglycones (− 7.8, − 8.1, − 8.2 kcal/mol for kaempferol, quercetin

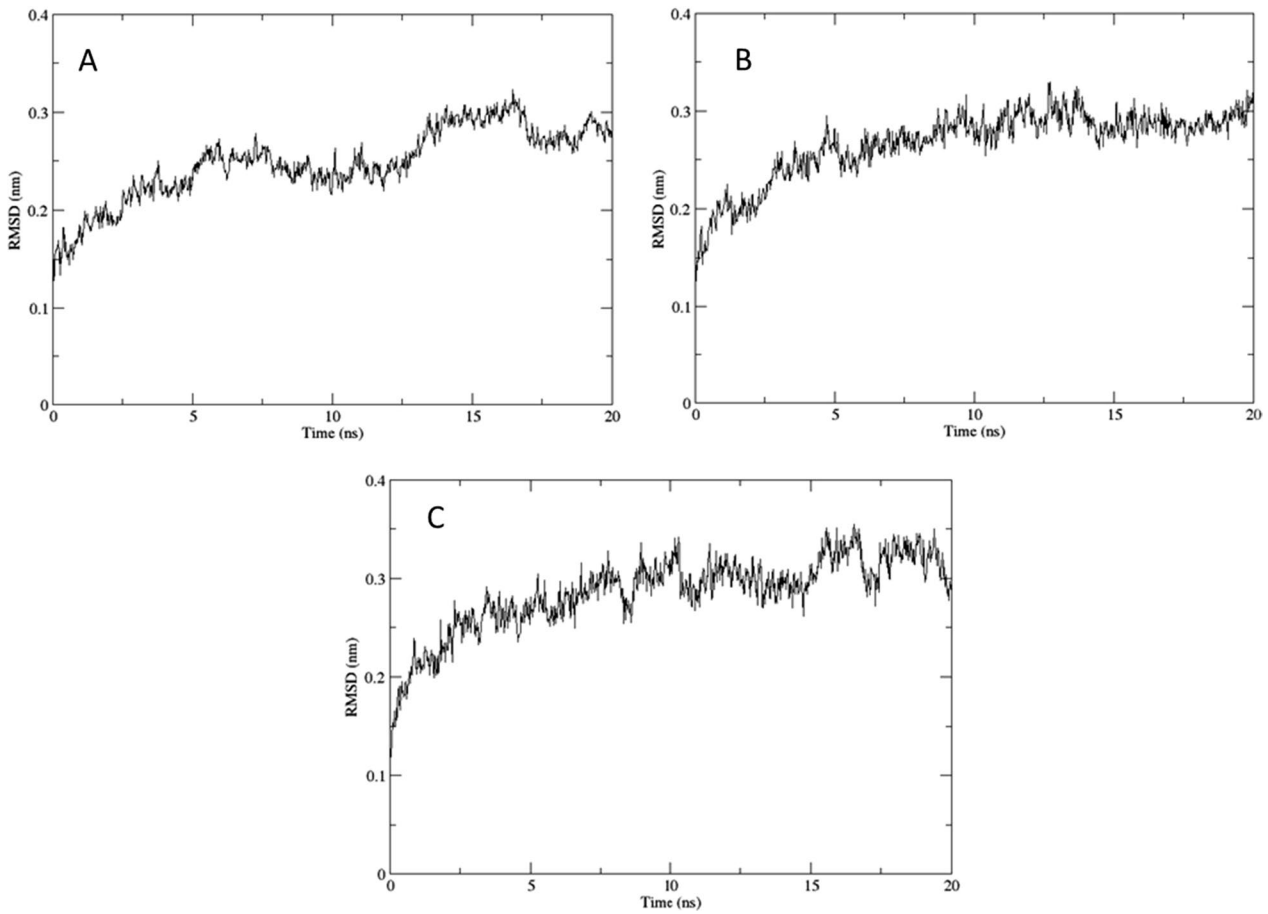

Fig. 11 RMSD curves showing instantaneous deviation of structures of: **A** isorhamnetin–XOD, **B** kaempferol–XOD and **C** quercetin–XOD complexes from their respective initial structures over a 20-ns simulation time

and isorhamnetin, respectively) were significantly lower than that of allopurinol (− 5.2 kcal/mol). This portends a higher binding affinity of each of the aglycones for XOD compared to that of allopurinol, projecting flavonoid aglycones as more-XOD specific than allopurinol and, invariably, indicating that more potent and safer uricostatics than allopurinol could emanate from the flavonoid aglycone chemical space [44].

Table 3 XOD inhibitory activities of isorhamnetin, quercetin and kaempferol calculated as inhibitory concentration producing 50% inhibition (IC_{50}) in µg/ml

Compound	IC_{50} (µg/ml)
Isorhamnetin	22.2 ± 2.1
Quercetin	20.4 ± 1.3
Kaempferol	8.2 ± 0.9
Allopurinol	30.1 ± 3.0

Molecular basis for the facility of flavonoid aglycone–XOD binding

The comparable in vivo activity of allopurinol and those of the flavonoid aglycones notwithstanding, molecular docking experiment results indicated that the flavonoid aglycones (FAs) showed more affinity to XOD than allopurinol did. The higher affinity of the FAs compared to allopurinol's could be speculated based on active site amino acid residues involved in their interactions as follows: Three active site amino acid residues (GLU1261, GLU802 and ARG880) have been recognized to be catalytically crucial to XOD biotransformation of xanthine to uric acid [45–47]. In addition, the active site bears other residues which, though non-catalytic, play significant roles in the purine substrate and cofactors binding. They include GLN767, PHE789, ARG912, ALA1079, PHE914 and THR1010 [37]. A careful analysis of the 2D and 3D active site interaction simulations of the aglycones (Figs. 7, 8 and 9) showed that each aglycone showed a pi-alkyl interaction with the substrate-binding ARG912,

while isorhamnetin, in addition, showed a carbon–hydrogen interaction with the rather catalytic GLU802. On the other hand, allopurinol's hydrogen bonding with THR1093 and pi-sigma bonding with GLN1040 (Fig. 6) were neither of substrate-binding nor of catalytic consequence, thereby explaining the higher binding affinities of the aglycones than that of allopurinol for XOD (Table 2). This, in a way, provides a strong molecular support for the possible discovery of potent anti-hyperuricemic agents from the flavonoid aglycones of TT and, by extension, the flavonoid aglycone chemical space in general.

Molecular dynamics of flavonoid aglycone–XOD complexes

Every atom in a physiological system is in a constant state of motion, being found in the field of forces exerted by surrounding atoms within and without the molecule of which it is a part [48]. Binding affinity outcomes of molecular docking would therefore often need to be validated by the stability of ligand–protein complexes in such dynamic environments simulated over a suitable period of time. Arguably, the two most useful stability-assessing parameters deductible from a typical ligand–protein complex dynamics simulation trajectory are radius of gyration (Rg) and root-mean-square deviation (RMSD) [48].

Rg is the time-based displacement of the coordinates of parts of the complex structure from a fixed point, usually its main axis. It specifically evaluates the compactness of the macromolecular structure or the proneness of its secondary structure to changes that could lead to folding perturbations and, hence, new tertiary structures, over a given period of time [48]. Rg values depend on the secondary structure of the protein involved. Predominantly, α-helix proteins tend to have higher Rg values than those of their β-sheet counterparts while those with mixtures of both have Rg values in between the two extremes [49]. Other critical factors affecting Rg values are the number of units the protein is made up of and the number of domains (or chains) making up each unit [49]. Analysis of the Rg-time plots of the aglycone–XOD complexes (Fig. 10) showed that each complex was largely maintained at an Rg below 28 Å, notably modest for an α-helix dominated huge (85 Kda) XOD C-terminal domain under consideration [50].

RMSD, in molecular dynamics parlance, is the deviation between the coordinates of atoms of a biomolecule at an instant and those of its initial structure. It is calculated by spatial rotation of an instantaneous structure to superimpose with the initial (or reference) structure with the maximum overlap possible. In other words, RMSD is a measure of deviation in the overlay of two compared structures, i.e. instantaneous and initial structures. It is used to assess the degree of conformational changes of the macromolecular structure in the course of the dynamics simulation [49]. RMSD-time plot of each aglycone–XOD complex (Fig. 11) showed the compared structures converging at around 2 ns, broadly plateauing for the rest of the 20 ns simulation time, with a deviation of instantaneous from initial structures averagely maintained around 3 Å during the period. This observation implies the general stability of the three aglycone–XOD complexes [51–53]. However, kaempferol–XOD complex demonstrated the least fine fluctuations associated with the RMSD plots particularly over the plateaued region, revealing it as the most stable of the three complexes. Molecular dynamics simulations therefore, in general, revealed a stable aglycone–XOD complex for each of the three flavonoid aglycones of TT and suggests kaempferol as a better inhibitor despite its least docking score (− 7.8 kcal/mol) compared to quercetin (− 8.1 kcal/mol) and isorhamnetin (− 8.2 kcal/mol).

In vivo XOD inhibition assay

The IC_{50} values of kaempferol (8.2 ± 0.9 µg/ml), quercetin (20.4 ± 1.3 µg/ml) and isorhamnetin (22.2 ± 2.1 µg/ml) were conspicuously lower than that of allopurinol (30.2 ± 3.0 µg/ml), showing that the three flavonoids are better XOD inhibitors than allopurinol, a standard XOD inhibiting antihyperuricemic drug. Further analysis of the IC_{50} values, however, showed that the three flavonoids do not have equal potencies, kaempferol (IC_{50}: 8.2 ± 0.9 µg/ml) being more potent than isorhamnetin and quercetin which have comparable potencies (IC_{50} 22.2 ± 2.1 µg/ml and 20.4 ± 1.3 µg/ml, respectively). This result is in tandem with the molecular dynamics simulation RMSD plots (Fig. 11) which showed kaempferol–XOD complex as more stable than the isorhamnetin–XOD and quercetin–XOD complexes. At this juncture, it is intellectually gratifying to speculate on the possible correlation of kaempferol's better-stabilized XOD complex and its associated stronger XOD inhibition potency to its distinct structure compared to those of isorhamnetin and quercetin: The three flavonoid aglycones are flavonols, essentially comprising a flavone skeleton with multiple oxygenated substituents, mostly hydroxyls (Fig. 2) [54]. Kaempferol, however, appears different from the other two in its lack of substitution at the 3′ position which is methoxylated and hydroxylated in isorhamnetin and quercetin, respectively. Recalling that each of isorhamnetin and quercetin showed unfavourable donor–donor interactions in the analyses of active site interaction simulations (Figs. 6, 7, 8 and 9), it is safe to link the lack of 3′ oxygenation in kaempferol to its lack of unfavourable active site interaction and hence the edge over its counterparts in XOD inhibition.

Conclusion

The current investigation, via in vivo SUA- and LUA-lowering data, vis-à-vis the adopted hyperuricemia induction protocol established the hyperuricemic potentials of TT, alluding its action mechanism to XOD inhibition corroborated by in silico molecular docking and molecular dynamics simulations. On another hand, the XOD inhibitory action mechanism has been confirmed by in vitro evaluation of the inhibitory activities of the three flavonoid aglycones of TT on a commercially available bovine XOD. The three flavonoid aglycones showed better inhibitory activity against the enzyme than allopurinol did both in vitro and in silico, portending the possible discovery of potent flavonoid-based uricostatic anti-hyperuricemic agents, using any of these flavonoids as a template. This investigation therefore unequivocally demonstrated the XOD-inhibiting antihyperuricemic activities of the flavonoid aglycone extract of *T. terrestris* and its three major flavonoid aglycones—isorhamnetin, quercetin and kaempferol. However, the role of synergism of these flavonoids in the activity of the extract and, hence, its possible application in combination therapy would require substantial additional data and hereby recommended as a further investigation.

Abbreviations

TT: *Tribulus terrestris*; UA: Uric acid; HUA: Hyperuricemia; FATT: Flavonoid aglycone-rich fraction of *Tribulus terrestris* leaf extract; MDS: Molecular dynamics simulation; RMSD: Root-mean-square deviation; Rg: Radius of gyration.

Acknowledgements

Not applicable.

Author contributions

OSA contributed to study design, data interpretation and manuscript writing; AOA did data collection and contributed to data interpretation and manuscript writing; MO contributed to study design, data interpretation and manuscript writing; MOA also contributed to study design and participated in data collection and manuscript writing; GU participated in data interpretation and manuscript writing. All authors proofread and approved the final manuscript.

Funding

This research did not receive any specific grant from funding agencies.

Availability of data and materials

Data are available and can be furnished upon reasonable request to the corresponding author (OSA).

Declarations

Ethics approval and consent to participate

The Lagos Health Research Ethics Committee of the College of Medicine of the University of Lagos (CMUL) approved the aspects of this study involving animal use (#CMUL/ACUREC/08/22/1076). The work did not involve any clinical trials. Consent to participate was therefore not applicable.

Consent for publication

Not applicable.

Competing interests

The authors declare that they have no competing interests.

Received: 8 October 2022 Accepted: 12 December 2022
Published online: 20 December 2022

References

1. Bardin T, Richette P (2014) Definition of hyperuricemia and gouty conditions. Curr Opin Rheumatol 26(2):186–191
2. Vargas-Santos AB, Neogi T (2017) Management of gout and hyperuricemia in CKD. Am J Kidney Dis 70(3):422–439
3. Indraratna PL, Williams KM, Graham GG, Day RO (2009) Hyperuricemia, cardiovascular disease, and the metabolic syndrome. J Rheumatol 36(12):2842–2843
4. Gliozzi M, Malara N, Muscoli S, Mollace V (2016) The treatment of hyperuricemia. Int J Cardiol 213:23–27
5. Kratzer JT, Lanaspa MA, Murphy MN, Cicerchi C, Graves CL, Tipton PA, Ortlund EA, Johnson RJ, Gaucher EA (2014) Evolutionary history and metabolic insights of ancient mammalian uricases. Proc Natl Acad Sci 111(10):3763–3768
6. Cao H, Pauff JM, Hille R (2010) Substrate orientation and catalytic specificity in the action of xanthine oxidase: the sequential hydroxylation of hypoxanthine to uric acid. J Bio Chem 285(36):28044–28053
7. Hille R, Nishino T (1995) Xanthine oxidase and xanthine dehydrogenase. FASEB J 9(11):995–1003
8. Nishino T, Okamoto K, Eger BT, Pai EF, Nishino T (2008) Mammalian xanthine oxidoreductase–mechanism of transition from xanthine dehydrogenase to xanthine oxidase. FEBS J 275(13):3278–3289
9. Enroth C, Eger BT, Okamoto K, Nishino T, Nishino T, Pai EF (2000) Crystal structures of bovine milk xanthine dehydrogenase and xanthine oxidase: structure-based mechanism of conversion. Proc Natl Acad Sci 97(20):10723–10728
10. Sattui SE, Gaffo AL (2016) Treatment of hyperuricemia in gout: current therapeutic options, latest developments and clinical implications. Ther Adv Musculoskelet Dis 8(4):145–159
11. Strilchuk L, Fogacci F, Cicero AF (2019) Safety and tolerability of available urate-lowering drugs: a critical review. Expert Opin Drug Saf 18(4):261–271
12. Corcoran MP, McKay DL, Blumberg JB (2012) Flavonoid basics: chemistry, sources, mechanisms of action, and safety. J Nutr Gerontol Geriatr 31(3):176–189
13. Ma Y, Zeng M, Sun R, Hu M (2014) Disposition of flavonoids impacts their efficacy and safety. Curr Drug Metab 15(9):841–864
14. Akram M, Asif HM, Akhtar N, Shah PA, Uzair MU, Shaheen G, Shamim T, Shah SA, Ahmad K (2011) *Tribulus terrestris* Linn.: a review article. J Med Plants Res 5(16):3601–3605
15. Semerdjieva IB, Zheljazkov VD (2019) Chemical constituents, biological properties, and uses of *Tribulus terrestris*: a review. Nat Prod Commun 14(8):1934578X19868394
16. Zhu W, Du Y, Meng H, Dong Y, Li L (2017) A review of traditional pharmacological uses, phytochemistry, and pharmacological activities of *Tribulus terrestris*. Chem Cent J 11(1):1–6
17. Mitra N, Mohammad-Mehdi D, Reza ZM (2012) *Tribulus terrestris* L. (Zygophyllaceae) flavonoid compounds. Int J Mod Bot 2:35–39
18. Nebieridze V, Skhirtladze A, Kemertelidze E, Ganzera M (2017) New flavonoid glycosides from the leaves of *Tribulus terrestris*. Nat Prod Commun 12(7):1934578X1701200714
19. Uric acid analysis assay kit. https://www.biolabo.fr/
20. UCSF Chimera 1.14, https://www.cgl.ucsf.edu/chimera/
21. BIOVIA Discovery studio visualizer (2021). https://discover.3ds.com/discovery-studio-visualizer-download
22. PyRx molecular docking software; https://pyrx.sourceforge.io/
23. University of Arkansas for Medical Sciences (UAMS) simlab webgro webserver; https://simlab.uams.edu/
24. RCSB Protein Databank; https://www.rcsb.org/
25. Pubchem; https://pubchem.ncbi.nlm.nih.gov
26. Computed Atlas of Surface Topography of proteins (CASTp); http://sts.bioe.uic.edu/
27. UniprotKB; https://www.uniprot.org/help/uniprotkb
28. PRODRG Webserver; http://davapc1.bioch.dundee.ac.uk/cgi-bin/prodrg

29. Dirir AM, Cheruth AJ, Ksiksi TS (2017) Ethnomedicine, phytochemistry and pharmacology of Calotropis procera and *Tribulus terrestris*. J Nat Remedies 17(2):38–47
30. Sofowora A (1993) Medicinal plants and traditional medicines in Africa. John Wiley & Sons, Chichester
31. Aniess W (2016) Effects of feeding some herbs on hyperuricemic rats. Nutr Bull 47(2):1–30
32. Adachi SI, Nihei KI, Ishihara Y, Yoshizawa F, Yagasaki K (2017) Anti-hyperuricemic effect of taxifolin in cultured hepatocytes and model mice. Cytotechnology 69(2):329–336
33. Adachi SI, Kondo S, Sato Y, Yoshizawa F, Yagasaki K (2019) Anti-hyperuricemic effect of isorhamnetin in cultured hepatocytes and model mice: structure–activity relationships of methylquercetins as inhibitors of uric acid production. Cytotechnology 71(1):181–192
34. Fossati P, Prencipe L, Betti G (1980) Use of 3,5-dichloro-2-hydroxybenzene sulfonic acid/4-aminophenazone chromogenic system in direct enzymatic assays of uric acid in serum and urine. Clin Chem 26:227–231
35. Jayaraja P, Bijo M, Parimaladevic B, Alex RV, Govindarajan R (2014) Isolation of a bioactive flavonoid from *Spilanthes calva* D.C. in vitro xanthine oxidase assay and *in silico* study. Biomed Prev Nutr 4(4):481–484
36. Umamaheswari M, Madeswaran A, Asokkumar K, Sivashanmugam T, Subhadradevi V, Jagannath P (2011) Study of potential xanthine oxidase inhibitors: *in silico* and in vitro biological activity. Bangladesh J Pharmacol 6(2):117–123
37. Abraham MJ, Murtola T, Schulz R, Páll S, Smith JC, Hess B, Lindahl E (2015) GROMACS: high performance molecular simulations through multi-level parallelism from laptops to supercomputers. SoftwareX 1(2):19–25
38. Yamamoto T, Moriwaki Y, Takahashi S (2005) Effect of ethanol on metabolism of purine bases (hypoxanthine, xanthine, and uric acid). Clin Chim Acta 356(1–2):35–57
39. Tang DH, Ye YS, Wang CY, Li ZL, Zheng H, Ma KL (2017) Potassium oxonate induces acute hyperuricemia in the tree shrew (*Tupaia belangeri* Chinensis). Exp Anim 66(3):209–216
40. Cao H, Pauff JM, Hille R (2014) X-ray crystal structure of a xanthine oxidase complex with the flavonoid inhibitor quercetin. J Nat Prod 77(7):1693–1699
41. Ho CY, Barr LG, Clifford AJ (1979) Immunological similarities of mammalian xanthine oxidases. Biochem Genet 17(3):209–221
42. Garattini E, Mendel R, Romão MJ, Wright R, Terao M (2003) Mammalian molybdo-flavoenzymes, an expanding family of proteins: structure, genetics, regulation, function and pathophysiology. Biochem J 372(1):15–32
43. Protein Data Bank (PDB) structure of bovine Xanthine Oxidase co-crystatlized with quercetin 3NVY, https://www.rcsb.org/structure/3nvy
44. Patrick GL (2013) An introduction to medicinal chemistry, 5th edn. University Press, Oxford
45. Ribeiro PM, Fernandes HS, Maia LB, Sousa SF, Moura JJ, Cerqueira NM (2021) The complete catalytic mechanism of xanthine oxidase: a computational study. Inorg Chem Front 8(2):405–416
46. Lin S, Zhang G, Pan J, Gong D (2015) Deciphering the inhibitory mechanism of genistein on xanthine oxidase in vitro. J Photochem Photobiol B Biol 153:463–472
47. Li Y, Kang X, Li Q, Shi C, Lian Y, Yuan E, Zhou M, Ren J (2018) Anti-hyperuricemic peptides derived from bonito hydrolysates based on in vivo hyperuricemic model and in vitro xanthine oxidase inhibitory activity. Peptides 107:45–53
48. Hollingsworth SA, Dror RO (2018) Molecular dynamics simulation for all. Neuron 99(6):1129–1143
49. Arnittali M, Rissanou AN, Harmandaris V (2019) Structure of biomolecules through molecular dynamics simulations. Procedia Comput Sci 156:69–78
50. Hille R (2006) Structure and function of xanthine oxidoreductase. Eur J Inorg Chem 10:1913–1926
51. Kumar N, Sood D, Tomar R, Chandra R (2019) Antimicrobial peptide designing and optimization employing large scale flexibility analysis of protein-peptide fragments. ACS Omega 4(25):21370–21380
52. Liu K, Watanabe E, Kokubo H (2017) Exploring the stability of ligand binding modes to proteins by molecular dynamics simulations. J Comput Aided Mol Des 31(2):201–211
53. Sargsyan K, Grauffel C, Lim C (2017) How molecular size impacts RMSD applications in molecular dynamics simulations. J Chem Theory Comput 13(4):1518–1524
54. Safe S, Jayaraman A, Chapkin RS, Howard M, Mohankumar K, Shrestha R (2021) Flavonoids: structure–function and mechanisms of action and opportunities for drug development. Toxicol Res 37(2):147–162

Publisher's Note

Springer Nature remains neutral with regard to jurisdictional claims in published maps and institutional affiliations.

Submit your manuscript to a SpringerOpen journal and benefit from:

- ► Convenient online submission
- ► Rigorous peer review
- ► Open access: articles freely available online
- ► High visibility within the field
- ► Retaining the copyright to your article

Submit your next manuscript at ► springeropen.com